DRAFT

Proceedings of ESDA2006
8th Biennial ASME Conference on Engineering Systems Design and Analysis
July 4-7, 2006, Torino, Italy

ESDA2006-95073

A VALIDATED CFD METHODOLOGY TO OBTAIN THE TOTAL PRESSURE LOSS COEFFICIENTS IN INTERNAL COMPRESSIBLE FLOW AT JUNCTIONS

J. Pérez-García, E. Sanmiguel-Rojas, J. Hernández-Grau and A. Viedma

Technical University of Cartagena. Department of Thermal and Fluid Engineering
C/ Doctor Fleming, s/n 30202 Cartagena, Spain
Tel: +34 968325986 Fax: +34 968 325999 E-mail: pepe.perez@upct.es

ABSTRACT

The 1-D models used in the global simulation of steady and transient compressible flow in pipe systems require reliable data of total pressure loss coefficients at singular elements such as junctions where the fluid flow is 3-D. These coefficients are usually introduced as boundary conditions. The characterization of these components of complex geometry can be carried out experimentally, analytically or, alternatively, through 3D numerical simulation.

In this work, a global methodology has been developed and validated to obtain the total pressure loss coefficient in internal compressible flow at T-type junctions. This methodology is based on the calculation of the thermo-fluid properties extrapolated to the branch axes intersection, once the straight pipe friction losses numerically calculated have been subtracted from the total energy losses. For this purpose, a steady adiabatic compressible one-dimensional flow with friction mathematical model has been applied to the results obtained by numerical simulation using the commercial finite volume code FLUENT to solve the steady state Navier-Stokes equations.

A 90 degree T-type junction has been studied and the predicted loss coefficient has been related to the extrapolated Mach number in the common branch and to the mass flow rate ratio between branches at different flow configurations, in both combining and dividing flows. The numerical results have been compared with experimental results and published data in open literature. In general, a good agreement is obtained. The correlations obtained will be applied as boundary condition in one-dimensional global simulation models of fluid systems in which these components are present.

INTRODUCTION

Nowadays steady and unsteady compressible internal fluid flow simulation models are essential in assisting the analysis and design of devices and plants where piping systems for gases and steam are required such as pneumatic fluid power systems, transport piping systems, inlet and exhaust systems in internal combustion engines and compressors and secondary air systems in gas turbines and rocket engines.

The 1-D models used in the global simulation of steady and transient compressible flow in pipe systems require reliable data of total pressure loss coefficients at singular elements such as junctions where the fluid flow is 3-D. These coefficients are usually introduced as boundary conditions. Different modelling techniques were compared by Basset *et al* [1] and they concluded that a wave action 1-D global simulation code, combined with 1-D loss pressure model to the T-type junctions provided satisfactory results with a lower computational cost against other more complex models for the junctions. Bulaty and Widenhorn [2] also proposed a similar model extended to multi-branch junctions. Chiatti and Chiavola [3] used a modelling technique based on the simultaneous use of zero, one and three-dimensional coupled models for the different regions along the exhaust system of a turbocharged engine. In addition, some commercial global

1-D simulation codes integrate a loss coefficient database, however these data are not available in open literature.

The characterization of these components of complex geometry can be carried out experimentally, analytically or, alternatively, through 3-D numerical simulation. There are numerous experimental data in incompressible flow in pipe junctions. The most reliable and complete reference data were obtained by Miller [4], these works and numerous experimental data from other authors were compiled in 73022 and 73023 ESDU [5][6]. Ito e Imai [7] also carried out an extensive test program at 90º pipe junctions. However, at present, the available information for compressible flow at junctions is limited and scarce. Besides, the published data are not sufficiently contrasted, they are obtained through a procedure that can be optimized, or they are restricted to a narrow range of Mach numbers. The most noticeable work corresponds to Benson *et al* [8], Dadone [9] and Morimune *et al* [10]. Abou-Haidar and Dixon [11] accomplished an extensive test program with T-type and Y-type junctions with different angles between branches and area ratios in a wide interval of Mach numbers. However, the procedure used to discount the frictional losses was based on the methodology defined by Miller [4], valid only for incompressible flow. This database is the most complete in open literature, but in order to be considered these coefficients as "class 1", according to Miller's classification, they should be contrasted.

Some analytical expressions to obtain the loss coefficient were also proposed by Abou-Haidar and Dixon [11], although the simplifications and assumed hypothesis such as inviscid and bi-dimensional fluid flow are too restrictive and in some flow configurations the results are not in a good agreement with the experimental data. Basset *et al* [12] extended the initial works of Hager [13] for all flow configurations in T-type and Y-type junctions, and they also proposed corrected analytical expressions for pulse-converter type junctions. A complete review is presented by Winterbone and Pearson [14].

The loss coefficient can also be predicted through 3D numerical simulation. The most noticeable works correspond to Leschziner and Dimitriadis [15], Fu et al [16], Kuo and Chang [17], Kuo and Khaligi [18], and Zhao and Winterbone [19]. They developed their own simulation codes based on finite-volume to obtain the loss coefficients. Other researchers, Shaw *et al* [20], Gan and Riffat [21] and Kesgin [22] used general purpose commercial codes such as Star-CD, Fluent or Fire-AVL respectively. Most of the works have been focused on the manifold design in ICE, and steady incompressible flow conditions were assumed in all cases. In consequence, an important lack of information related to the determination of loss coefficient by numerical simulation in 3D compressible flow has been detected. Besides, detailed information about internal structure of the flow inside junctions focused to basic research can be achieved by this technique.

In incompressible flow the traditional loss coefficient used in previous works cited above are based in Miller's definition [4]. For compressible flow Miller [23] proposed a loss coefficient defined as the ratio between the total pressure losses and the dynamic pressure in the common branch by analogy with the definition used in incompressible flow. This definition was used later by Abou-Haidar and Dixon and other authors. Usually, the loss coefficient is represented against the extrapolated Mach number in common branch, taking into account that the extrapolated quantities are the fluid properties calculated at the junction once the friction losses have been subtracted from the total energy losses of the fluid flow. Most of 1-D global simulation codes directly use the loss coefficient or correlations with other parameters as boundary conditions. The flow behaviour at junctions can also be characterized by a discharge coefficient or a flow coefficient. Other authors as Kesgin [22] or Christian *et al* [24] have proposed their loss coefficient definitions.

In summary, there is not enough available and reliable data in open literature about total pressure loss coefficients at junctions for compressible flow. In the present work, a global methodology developed to obtain the total pressure loss coefficient in compressible flow at junctions through numerical simulation is exposed. The commercial package software Fluent is used in this study.

The developed methodology is based on the calculation of the thermofluid properties extrapolated to the geometrical junction, once the frictional losses have been subtracted from the total energy losses. An adiabatic compressible steady one-dimensional flow mathematical model has been applied for this purpose. The procedure has been validated comparing the numerical results obtained in a 90 deg T-type junction with own experimental results and published reference data. In this paper, the numerical results obtained for combining and dividing flow type configurations and three different mass flow rate ratios between branches are presented. The loss coefficient has been related with the extrapolated Mach number in the common branch.

NOMENCLATURE

D	Internal diameter (m)
f	Fanning Friction factor (dimens.) $f = \tau_w / \frac{1}{2}\rho u^2$
f_D	Friction factor (dimensionless) $f_D = 4f$
h_0	Stagnation enthalpy (J/kg)
h	Static enthalpy (J/kg)
K	Total pressure loss coefficient defined by Miller (dimensionless)

L/D	Non-dimensional distance (distance related to internal diameter)
G	Mass flow rate (kg/s)
M	Mach number (dimensionless) $M = U/a$
p_0	Stagnation pressure (Pa)
p	Static pressure (Pa)
p_t	Total pressure (Pa) $p_t = p + \frac{1}{2}\rho u^2$
q	Mass flow rate ratio between branches (dimensionless) $q = G_2/G_3$
S	Cross-sectional area (m^2)
T_0	Stagnation temperature (K)
T	Static temperature (K)
ϕ_j	Ratio of extrapolated absolute static pressure (dimensionless) $\phi_j = p_j^*/p_3^*$
u_i	Gas velocity components $i = 1,2,3$ (m/s)
u_i'	Fluctuating velocity components (m/s)
x	Distance along each branch (m)
y^+	Sublayer scaled distance (dimen.) $y^+ = u_\tau y/\nu_w$
ε	Non-dimensional roughness
ϕ_v	Rayleigh dissipation function (Pa/s)
γ	Ratio of specific heats (dimensionless) $\gamma = c_p/c_v$
μ	Absolute viscosity (Pa.s)
ρ	Gas density (kg/m^3)
τ_w	Wall shear stress (Pa) $\tau_w = \rho u_\tau^2$
τ_{eff}	Apparent stress tensor (Pa)

Subscripts

1,2	Inlet (comb. flows), outlet (bif. flows) branches
3	Common branch
*	Extrapolated fluid properties to the junction
D	Dividing flow
C	Combining flow
i	Test section in each branch $i = 1, 2, ... N$
j	Branch $j = 1, 2, 3$

1. Global Methodology

1.1 Mathematical Model

The fluid flow studied is governed by 3D compressible adiabatic steady-state form of the Reynolds-Averaged Navier-Stokes (RANS) conservation equations and the additional equations describing the transport of other scalar properties. They may be written in Cartesian tensor notation as:

$$\frac{\partial}{\partial x_i}(\rho u_i) = 0 \quad (1)$$

$$\frac{\partial}{\partial x_i}(\rho u_i u_j) = -\frac{\partial p}{\partial x_i} + \frac{\partial}{\partial x_j}\left[\mu\left(\frac{\partial u_i}{\partial x_j} + \frac{\partial u_j}{\partial x_i}\right) - \frac{2}{3}\mu\delta_{ij}\frac{\partial u_k}{\partial x_k}\right] \quad (2)$$

$$\ldots + \frac{\partial}{\partial x_j}\left(-\rho\overline{u_i' u_j'}\right) = -\frac{\partial p}{\partial x_i} + \frac{\partial}{\partial x_j}\bar{\tau}_{eff}$$

$$\frac{\partial}{\partial x_i}(u_i h_0) = \frac{\partial}{\partial x_j}\left(u_i \bar{\tau}_{eff}\right) = u_i \frac{\partial}{\partial x_j}\bar{\tau}_{eff} + \Phi_v \quad (3)$$

In order to model the Reynolds stresses and the turbulent diffusivity terms, different turbulence models based on RANS equations can be used. In this work the two equations turbulent model $k-\omega$ SST (Shear-Stress Transport) Menter [25] will be used. The main characteristic of this turbulent model is that the eddy viscosity is redefined so as to take into account the transport of the principal turbulent shear stress Wilcox [26].

The wall boundary conditions in the $k-\omega$ models are treated in the same way as when enhanced wall treatments are used with the $k-\varepsilon$ models. So all boundary conditions for wall-function meshes will correspond to the wall-function approach, while for the fine meshes, or when the $y^+ \leq 30$, the appropriate low-Reynolds-number boundary conditions will be applied. Different turbulent models and their respective options, implemented in Fluent, were compared. In section 1.3.2.2 a comparative study is presented.

1.2 Flow Configurations. Definition of Total Pressure Loss Coefficient at Junctions

In general six flow configurations can take place at asymmetrical T-type junctions, three dividing flow types (D1, D2 and D3) and an other three in combining flow (C1, C2 and C3). In consequence, twelve loss coefficients can be defined. At symmetrical 90 degree T-type junctions the flow types are reduced to four possible flow configurations (figure 1). In this case, five mass flow rate ratios between branches $q = 1, 0.75, 0.5, 0.25$ and 0 have been simulated in each flow type.

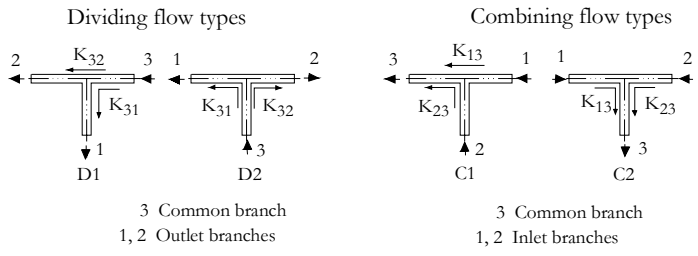

Figure 1. Flow configurations studied

The total pressure loss coefficient defined by Miller [23], equations (4), and used by Abou-Haidar and Dixon, has also been used in this study to accomplish the comparisons. This coefficient is defined, likewise to the coefficient in incompressible flow, as the ratio of the stagnation pressure losses between common branch and the inlet or outlet branch, to the difference between stagnation and static pressure in the common branch. Dimensional analysis allows us to deduce that the loss coefficient is a function of mass flow rate ratio "q" and extrapolated Mach number in common branch M_3^*, $K = f(q, M_3^*)$. Since, according to the results of different previous researchers the influence of Reynolds number, based on duct diameter, is negligible on the loss coefficient in sharp-edged T-type junctions when $\mathrm{Re}_D > 10^5$.

$$K_{3j} = \frac{p_{03}^* - p_{0j}^*}{p_{03}^* - p_3^*} \quad \text{(D1, D2)} \qquad K_{j3} = \frac{p_{0j}^* - p_{03}^*}{p_{03}^* - p_3^*} \quad \text{(C1,C2)} \quad (4)$$

$$j = 1,2$$

The main disadvantage of this coefficient is the low sensitivity to Mach number such as it will be showed in section 3.2, and the propagation of the measurement uncertainty, that it can be about ±25%, in some flow types, when the errors in the static pressure measurements is about 1%.

1.3 Computational Domain and Simulation Hypothesis

1.3.1 Computational Domain

A structured, non-uniform mesh has been built. In figure 2, a detail of the grid in the intersection of the branches region, the mesh structure on the symmetry plane and a detail of the mesh at the cross-section are shown. The mesh was generated through preprocessing software Gambit. Due to the symmetry of the 90 degree T-type junction, in all flow configurations the computational domain can be considered one half of the actual volume. Additionally, in $C2$ and $D2$ flow types, the simulations can be accomplished for a quarter of the total volume when $q = 0.5$, which saves time and computational efforts.

In order to ensure accuracy of the predictions a grid dependence study was performed. Simulations were carried out for different computational meshes, modifying the distance of the wall-adjacent cells to the wall. Through a mesh refinement process by Fluent, the y^+ value is maintained within the recommended range for all mass flow rates simulated. The number of cells of the mesh finally used was 176,832 and the required computational time for each case is about one week in a workstation Compaq HPC160 16 processor 1 GHz.

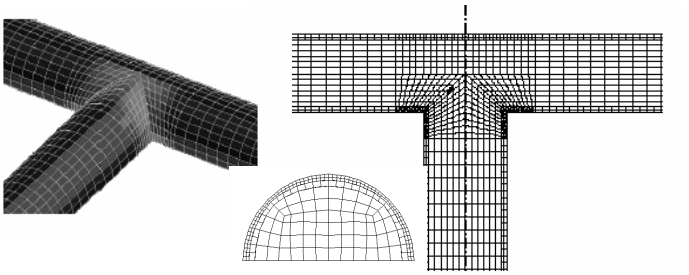

Figure 2. 3D Computational domain and mesh structure in the plane of symmetry and in the cross-sectional of a branch at T-type junction simulated

All branches have a circular cross-section and the same diameter and length. The intersection is sharp-edged. The length of the branches is an important choice since fully developed flow condition upstream and downstream in the junction influence region must be reached at the inlet and outlet branches; otherwise the one-dimensional model is not suitable. Also, it must be taken into account that the frictional effect limits the maximum mass flow rate. In this way, when the length is increased the range of extrapolated Mach number is decreased. This is one of the problems found during the experimental test since the location of the measurement section must be carefully chosen so that the flow is fully developed.

Simulations have been accomplished to, $50D$, $100D$ and $200D$ branch length meshes, concluding that the total pressure loss coefficient is kept constant for equal extrapolated Mach numbers, whatever the length of the branches, although to achieve high subsonics Mach numbers short outlet branches are required. However, outlet branches which are too short can yield loss coefficients of low reliability.

1.3.2 Simulation Hypothesis

1.3.2.1 Solver

The governing equations are solved using the commercial finite volume code FLUENT [27]. The convective terms are discretized using a second-order upwind scheme. Fluent implements two different solvers: the coupled solver with "implicit" and "explicit" formulations and the segregated solver. In the coupled solver the momentum and energy equations are solved simultaneously, while the segregated solver solves these equations sequentially. The implicit and explicit coupled solvers differ in the way that they linearize the coupled equations. In compressible flow the coupled solver is required, although the computational cost is greater and the convergence is more difficult to achieve.

In figure 3, the numerical results obtained using $k-\omega$ SST turbulence model with both segregated and coupled implicit solvers are showed and compared with

experimental data for combining flow type $C2$ and $q = 0.5$. It can be observed that numerical results using the coupled solver are in better agreement with experimental and reference data, that those obtained using the segregated solver, regardless of the turbulence model used. In consequence, all simulations have been carried out with coupled implicit solvers.

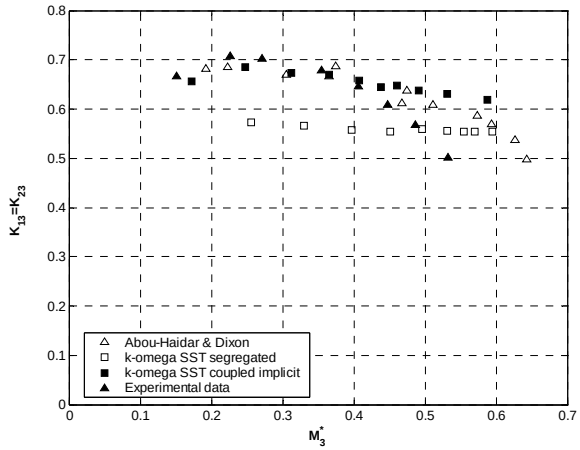

Figure 3. Comparison between segregated and coupled solvers. Flow type $C2$ $q = 0.5$

1.3.2.2 Turbulence Model

Different turbulent models implemented in Fluent have been compared. The $k-\varepsilon$ "standard" with "standard wall functions" and "realizable" with "non-equilibrium wall functions", $k-\omega$ "standard" and "SST" and Spalart-Allmaras turbulence models have been used in preliminary simulations at different flow configurations. The "RSM" model has been discarded due to high computational efforts required. The $k-\omega$ "SST" with "compressibility effects" option, $k-\varepsilon$ "realizable" with non-equilibrium wall functions and Spalart-Allmaras are recommended in wall-bounded flows involving recirculation zones and adverse pressure gradient. These characteristics are present in the internal fluid flow at junctions.

In figures 4 and 5, the total pressure loss coefficients obtained with each turbulence model are represented against an extrapolated Mach number in common branch, M_3^* at flow types $C2$ and $D2$ with $q = 0.5$ and compared with experimental and reference data. It can be observed that in the combining flow type $C2$ (figure 4), the loss coefficient predicted by the different turbulence models is similar in all cases and are in a good agreement with experimental and reference data. However, in the dividing flow type $D2$ (figure 5), the discrepancies among the different turbulence models are valuable. The numerical results are in general in satisfactory agreement and it can be concluded that the loss coefficient predicted using the $k-\omega$ "SST" turbulence model is the most suitable in this flow type. In consequence, this last turbulence model will be used in all numerical simulations.

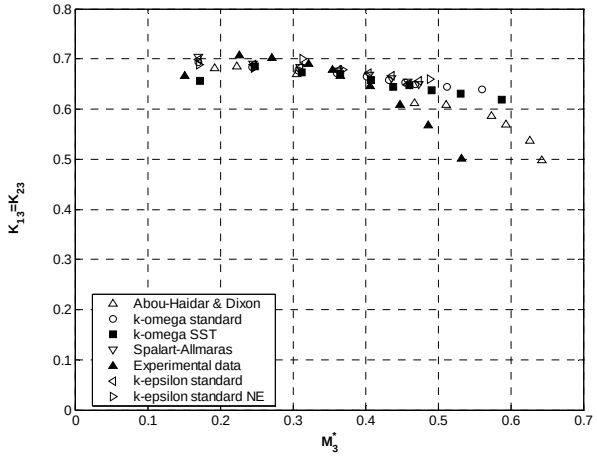

Figure 4. Comparison among different turbulence models. Flow type $C2$ $q = 0.5$

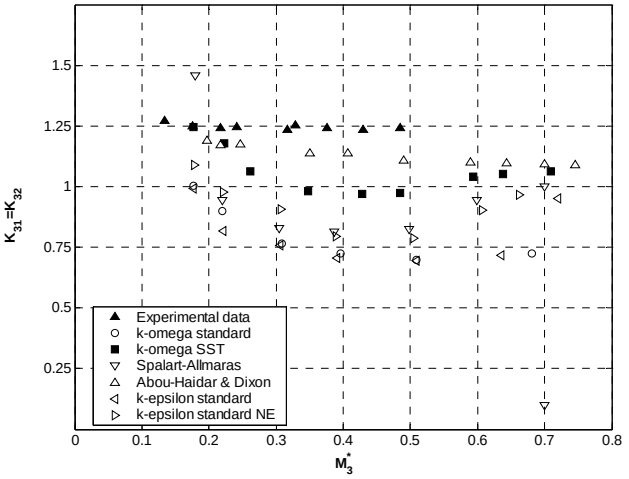

Figure 5. Comparison among different turbulence models. Flow type $D2$ $q = 0.5$

1.3.2.3 Boundary Conditions and Fluid Properties

In combining flow types at the inlet boundary locations a mass flow rate was fixed, while the static pressure was set at the outlet boundary locations. In dividing flow types the target-mass-flow-rate option is turned on to impose the mass flow rate ratio between branches. In both the turbulence intensity and the hydraulic diameter were set to 4% and 0.012 respectively as turbulence parameters. At the walls, the usual non-slip condition, adiabatic flow and wall roughness height was prescribed. This means that a modified wall function for roughness will be applied. Ideal gas law for density, specific heat constant and Sutherland equation for the molecular viscosity are used to define the fluid properties.

1.4 Numerical Processing Methodology

The numerical processing methodology to obtain the loss coefficient consists in the following steps:

a) To obtain the average static temperature $T_i \equiv \overline{T}(x_i)$ from (5) in the cross-sectional area $S_i \equiv S(x_i)$ at the different locations x_i from the intersection, in the three branches.

$$\overline{T}(x_i) = \frac{1}{S_i}\int_{S_i} T(x_i, y, z)dS_i \tag{5}$$

The stagnation temperature $T_{0i} \equiv \overline{T}_0(x_i)$ is constant along each branch, due to the imposed adiabatic flow conditions.

b) To calculate the average Mach number $M_i \equiv \overline{M}(x_i)$ at the different locations from (6) in each branch.

$$\overline{T}_0(x_i) = \overline{T}(x_i)\left[1+\frac{\gamma-1}{2}\overline{M}^2(x_i)\right]^{1/2} \tag{6}$$

c) To calculate the friction coefficient $f_{Di} \equiv f(x_i)$ from numerical integration of momentum equation in one-dimensional steady compressible and adiabatic flow conditions (7), in the three branches. The flow type, mass flow rate ratio between branches q, and number of locations n must be taken into account.

$$f_{Di} = \frac{2D}{\gamma M_i^3}\frac{1-M_i^2}{1+\frac{1}{2}(\gamma-1)M_i^2}\left.\frac{dM}{dx}\right|_i \tag{7}$$

To discretize $dM/dx|_i$ in a non-uniform grid by finite differences, equations exposed in Sanmiguel-Rojas *et al* [28] have been used.

In figure 6 a) the friction coefficient from (7) is represented. An intermediate zone can be observed in which the friction coefficient reaches a constant value, and, in consequence, the flow is fully-developed and the hypothesis of Fanno flow is achieved. However, near the intersection, large changes in f_D are originated by the junction effect and the 1D model is not valid. The amplitude of this three-dimensional region mainly depends on mass flow rate and flow type. In the end of the branch the friction coefficient is influenced by the numerical boundary condition and this adaptation length must be suppressed in the processing. This information allows us to fix the required distance in each branch between the measurement location and the junction. So, the friction coefficient numerically calculated is more accurate than experimentally, due to the most complete information about the magnitude gradients provided by numerical simulations. In the experimental measurement a correlation must be used, assuming fully developed flow.

d) To calculate the extrapolated Mach number up to the intersection M_j^*, $j = 1,2,3$, from each location x_i using the equation (8). This equation is obtained by analytical integration of (7) assuming a previously calculated local constant friction coefficient in c).

$$f_{Di}\frac{(x_i - x_{i-1})}{D} = \frac{1}{\gamma M_i^2}\left(\frac{M_i^2 - M_{i-1}^2}{M_{i-1}^2}\right) + \frac{\gamma+1}{2\gamma}\ln\left[\frac{M_{i-1}^2\left(2+(\gamma-1)M_i^2\right)}{M_i^2\left(2+(\gamma-1)M_{i-1}^2\right)}\right] \tag{8}$$

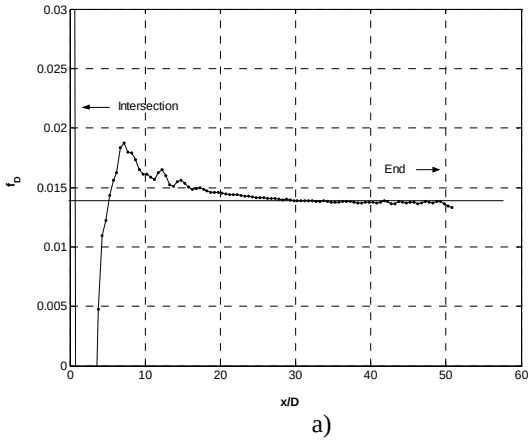

a)

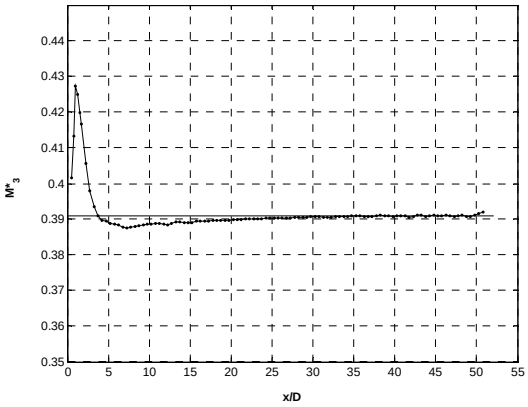

b)

Figure 6. Friction coefficient f_D in a) and extrapolated Mach number in b) for the common branch. Flow type $C2$ $q = 0.5$ $G_3 = 0.08$ kg/s

In figure 6 b), the extrapolated Mach number is represented. A constant value can be observed far from the region influenced by the junction.

e) Once the extrapolated Mach number for each branch has been obtained, all thermo-fluid properties extrapolated can be calculated and the total pressure loss coefficient computed from the equations (4).

2.1 Experimental Test

2.1.1 Flow Facility

The experimental tests have been conducted in a flow bench. This facility mainly consists in a 36.8 kW

screw compressor and a conditioning air system formed by two reservoirs, a pressure regulator, a filtering line and an air dryer. The flow bench also includes three Coriolis effect mass flow-meters and a pipe network with the necessary control valves to establish the flow configurations and the mass flow rate ratio between branches during the junction tests. The maximum mass flow rate supplied is 0.12 kg/s of dried air at about 0.8 MPa.

The static absolute pressure was measured by extensiometric transmitters, and the static air temperature by means of calibrated T-type thermocouples. The mass flow rates were measured at two branches upstream or downstream at the junction, according to flow configuration. The static drop pressure between common branch and the other branches were measured by means of a differential piezoresistive pressure transmitter. The output signal of mass flow rate meters, absolute and differential pressure transmitters and thermocouples were connected to a digital multimeter HP 34970A.

2.1.2 Geometrical Characteristics of Tested Junction

In figure 7, the arrangement for a combining flow test is depicted. The tested 90 degree T-type junction has a circular cross-sectional area. The internal diameter in all branches is 12 mm and their inner surface roughness is about 1 μm. The axes are coplanar and the intersections are sharp-edged. A flow-rate regulator device and a flow straightener followed by a straight duct of $10D$ length and a nozzle ensure that the flow entering was fairly uniform and the interactions that would take place with other components or fittings are minimized. The nozzle was followed by a straight length of $20D$ upstream of the measurement location. The distance between the measurement points and the junction was about $35D$.

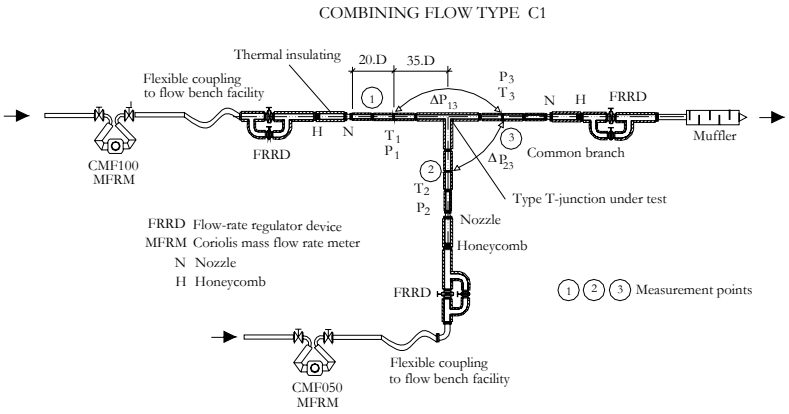

Figure 7. Arrangement of the experimental setup

It is important to emphasize that one of the most complex aspects in compressible flow measurement is to achieve fully developed fluid flow conditions with shortest branch lengths since the friction coefficient can be substantially modified. On the other hand, branches that are too long can yield choked flow due to friction effects, which limits the Mach number interval tested. The junction under test was modular and all branches were thermally insulated to guarantee adiabatic flow conditions.

2.1.3 Experimental Data Processing

Experimental data were acquired for the four possible flow configurations. The mass flow rate ratio between branches were fixed at $q = 0$, 0.2, 0.25, 0.4, 0.5, 0.6, 0.75, 0.8 and 1 at each flow type. In all cases, the thermo-fluid properties measured in
each branch were reduced and processed for different mass flow rates.

The experimental data processing procedure consists in the following steps:

a) To calculate the mass flow rate ratio and consistence analysis of the measurement
b) To calculate the extrapolated thermo-fluid properties

b.1) To obtain the friction coefficient departing from Reynolds number and non-dimensional roughness. The von Karman-Nikuradse or Colebrook-White correlations can be used according to the mass flow rate. The absolute viscosity is obtained from Sutherland´s equation and gas density from ideal gas law corrected with compressibility factors. The ratio of specific heats and the specific heat at constant pressure is considered as function of the temperature

$$\begin{cases} \mathrm{Re}_{Di} = \dfrac{\rho_i U_i D_i}{\mu_i} \\ \varepsilon = \dfrac{k}{D} \end{cases} \rightarrow \begin{cases} \dfrac{1}{\sqrt{f_{Di}}} = 2\log_{10}\left(\mathrm{Re}_{Di}\sqrt{f_{Di}}\right) - 0{,}8 \\ \dfrac{1}{\sqrt{f_{Di}}} = -2\log_{10}\left(\dfrac{k/D}{3{,}7} + \dfrac{2{,}51}{\mathrm{Re}_{Di}\sqrt{f_{Di}}}\right) \end{cases} \quad (9)$$

b.2) Once the frictional coefficient is obtained, the steady one-dimensional adiabatic flow model is applied and the gas velocity relation (U_i/U_{i+1}) from equation (10) can be calculated in each section. Later, the pressure relation (p_{i+1}/p_i) is calculated from equation (11)

$$\bar{f}_{Di}\frac{L}{D} = \frac{1}{\gamma M_i^2}\left(1+\frac{\gamma-1}{2}M_i^2\right)\left[1-\left(\frac{U_i}{U_{i+1}}\right)^2\right] + \frac{\gamma+1}{2\gamma}\ln\left[\left(\frac{U_i}{U_{i+1}}\right)^2\right] \quad (10)$$

$$\frac{p_{i+1}}{p_i} = \frac{U_i}{U_{i+1}}\left\{1+\frac{\gamma-1}{2}M_i^2\left[1-\left(\frac{U_{i+1}}{U_i}\right)^2\right]\right\} \quad (11)$$

b.3) Departing from U_{i+1}, p_{i+1} and mass flow rate, all thermo-fluid properties can be obtained and the next section will be calculated. Once the intersection is reached

the extrapolated properties $U^*, P^*, T^*, M^*, P_o^*$ in all branches are known and the total pressure loss coefficient can be calculated from equations (4).

The experimental determination of the pressure loss coefficient as a function of mass flow rate ratio and extrapolated Mach number in common branch entails an expanded uncertainty mainly due to measurements errors and their propagation according to the definition of the coefficient and to the errors due to the non-uniformity and non-fully developed flow in the measurement sections. The results of expanded uncertainty calculation under ISO standard "Guide to the Expression of Uncertainty in Measurement" [29] are about 2% for the mass flow rate ratio between branches and Mach number and up to about 25% for the total pressure loss coefficient, depending on the flow configuration.

3. Results and Discussion

The total pressure loss coefficient obtained using the developed methodology are represented in two ways, in incompressible form, as a function of flow rate ratio q when $M_3^* \leq 0.2$, and as a function of extrapolated Mach number in common branch, M_3^* in compressible flow.

The Reynolds number interval reached during the numerical simulations and experimental test was about $1.10^5 \leq \mathrm{Re} \leq 7.10^5$. In this range the loss coefficient can be assumed independent of this parameter according to different authors. The maximum attainable extrapolated Mach number is dependent of several factors, such as branch length, frictional losses, flow separation and "vena contracta" phenomena…etc.

In the following figures, the comparisons with the available data in open literature and experimental results obtained in flow bench are showed for the combining $C2$ and dividing $D2$ flow types. At combining flow types, the extrapolated Mach number interval experimentally reached was $0.1 \leq M_3^* \leq 0.6$, in this configuration the maximum Mach number is mainly limited by the flow separation and the reduction of effective area (vena contracta) at common branch entrance causing choked flow conditions. At dividing flow types, the interval is reduced to $0.1 \leq M_3^* \leq 0.5$ due to the requirements of the experimental arrangements. This interval can be extended in the numerical simulations, most specially in dividing flow types.

3.1 Comparison between Numerical and Experimental Results in Incompressible Flow

In this section the loss coefficient values obtained to extrapolated Mach numbers $M_3^* \leq 0.2$ are compared with different reference data. In figure 8, the total pressure loss coefficients obtained at $C2$ and $D2$ flow type both experimentally and numerically are compared with the available reference data. It can be observed in general a good agreement. However, the loss coefficient definition is different in many references. So, when the incompressible form is used to correlate the loss coefficient, this is usually obtained from equations (12).

$$K_{3j} = \frac{p_{t3}^* - p_{tj}^*}{\frac{1}{2}\rho \bar{U}_3^2} \text{ (D1, D2)} \qquad K_{j3} = \frac{p_{tj}^* - p_{t3}^*}{\frac{1}{2}\rho \bar{U}_3^2} \text{ (C1, C2)} \quad (12)$$

$$j = 1,2$$

At $C2$ combining flow type the experimental data is close to reference data for all flow rate ratios, excluding the Benson and Woollatt data, these discrepancies can be due to the short distance from the location measurement up to the junction in their tests and to the influence of friction losses. It is noticeable that in the ESDU data compilation the fluid used in test was water, while air was used by Abou-Haidar and Dixon and Dadone. In this last case, the loss coefficient was obtained for different Mach numbers maintained constant.The numerical simulations were accomplished for $q = 1, 0.75, 0.5, 0.25 \text{ and } 0$ in the incompressible range. In all cases the numerical results are in satisfactory agreement, taken into account the expanded uncertainty of the loss coefficient . Although, the loss coefficient obtained at $q = 0$ is not fully reliable, since when the mass flow rate is null, the y^+ is out of the interval recommended by Fluent, however the loss coefficient is accurately predicted. At $q = 1$ the loss coefficient is slightly underestimated.

At $D2$ dividing flow type the experimental results are in good agreement, although in this flow type, larger data dispersion can be expected because an unstable flow pattern can be developed which causes large increases in the loss coefficient according to ESDU. The numerical results are in accordance with reference and experimental data at $q = 1, 0.75, 0.5 \text{ and } 0.25$. However, the loss coefficient obtained at $q = 0$ is in disagreement. These discrepancies can be due to errors in the numerical simulation model, it seems that it cannot be able to predict the suction effect in the branch without mass flow rate. In this case, a direct numerical simulation (DNS) would be used, although due to the great computational cost required, it is actually out of our reach.

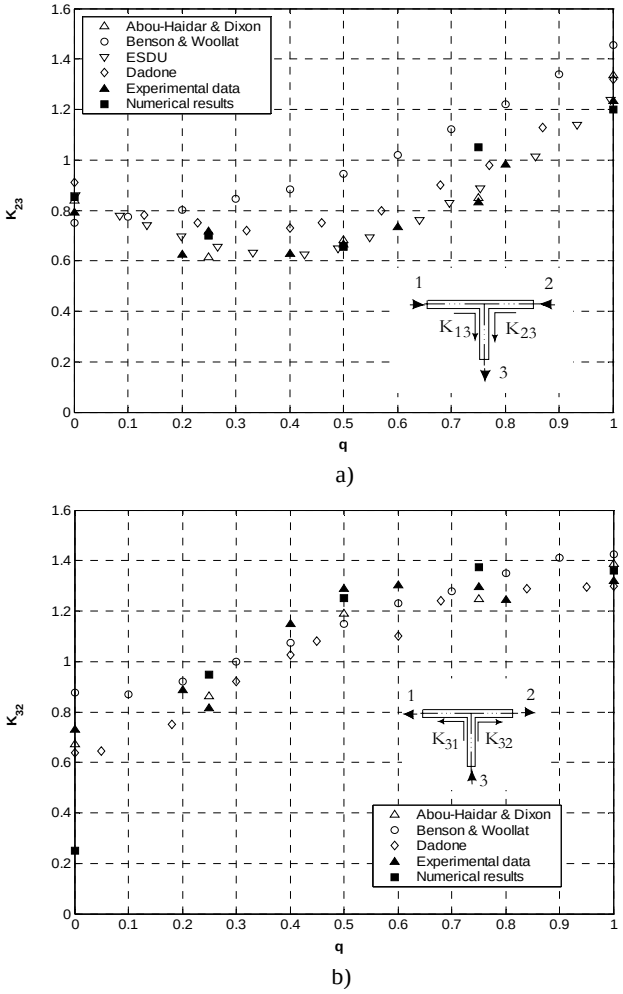

Figure 8. Comparison among reference data, experimental data and numerical results for different flow ratios.a) Loss coefficient K_{23} *(*K_{13} *considering* $1-q$*) for combining flow type* $C2$ *b) Loss coefficient* K_{32} *for dividing flow type* $D2$

3.2 Comparison in Compressible Flow

The obtained experimental and numerical results have been compared with Abou-Haidar and Dixon's published data, in order to validate the methodology developed. To accomplish these comparisons the loss coefficient defined by Miller has been calculated for different flow configurations and mass flow rate ratio between branches and has been represented as a function of extrapolated Mach number in common branch, maintaining the mass flow rate ratio as a constant parameter. These parameters are used to characterize the loss coefficient in steady compressible flow at junctions, since, according to the dimensional analysis $K_{3j} = \varphi\left(q, M_3^*\right)$ at high Reynolds number $\left(\mathrm{Re} > 1.10^5 \div 1.10^6\right)$.

The four possible flow configurations at symmetrical 90 degree T-type junctions studied have been analyzed and five mass flow rate ratios between branches $q = 1, 0.75, 0.5, 0.25 \text{ and } 0$ have been numerically simulated and experimentally tested in each flow type. In general, the loss coefficient defined from equation (4) and used in this work presents a low variation with the Mach number. It must also be taken into account that the procedure followed to subtract the frictional losses in the experimental results differs in reference to the method used by Abou-Haidar and Dixon. Therefore some discrepancies between experimental results and reference data can be expected.

3.2.1 Combining Flow Type $C2$

The maximum averaged Mach number value attainable in this case is about 0.6. This restriction is due to the "*vena contracta*" phenomenon and the blockage effect of the cross-section caused by the flow separation at the inlet in the common branch. The numerical results allow us to visualize the Mach number contours in this zone, in which the local Mach number reaches the sonic condition, as shown in figure 9. The branch length will also limit the maximum mass flow rate and the extrapolated Mach number due to the frictional effects.

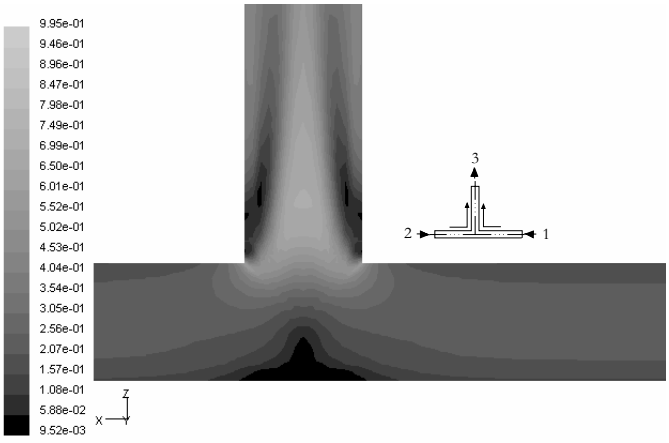

Figure 9. Contour of Mach number at symmetry plane. Flow type $C2$ $q = 0.5$ $G_3 = 0.176$ *kg/s* $\bar{p}_{outlet} = 400$ *kPa*

In figure 10, the obtained total pressure loss coefficients K_{23} are represented for different mass flow rate ratios . It can be observed that the loss coefficient defined by Miller presents a low variation with the extrapolated Mach number. The trends are similar in all cases, and the loss coefficients are, in general, in a good agreement, mainly at low Mach numbers. At $q = 0.5$ $K_{13} = K_{23}$ and the results are coincident below $M_3^* = 0.5$, however at higher Mach numbers some discrepancies are encountered. These discrepancies can be due to the loss coefficient definition and to the differences in the processing methodology. In addition, at a higher Mach number the fluid flow could not be uniform in the measurement location downstream of the flow intersection, and in consequence, errors in the calculation of friction coefficient can be produced. This error is minimized with the numerical results, because complete information on the evolution of magnitude gradients with the non-dimensional distance is available and an accurate value of the friction coefficient can be calculated.

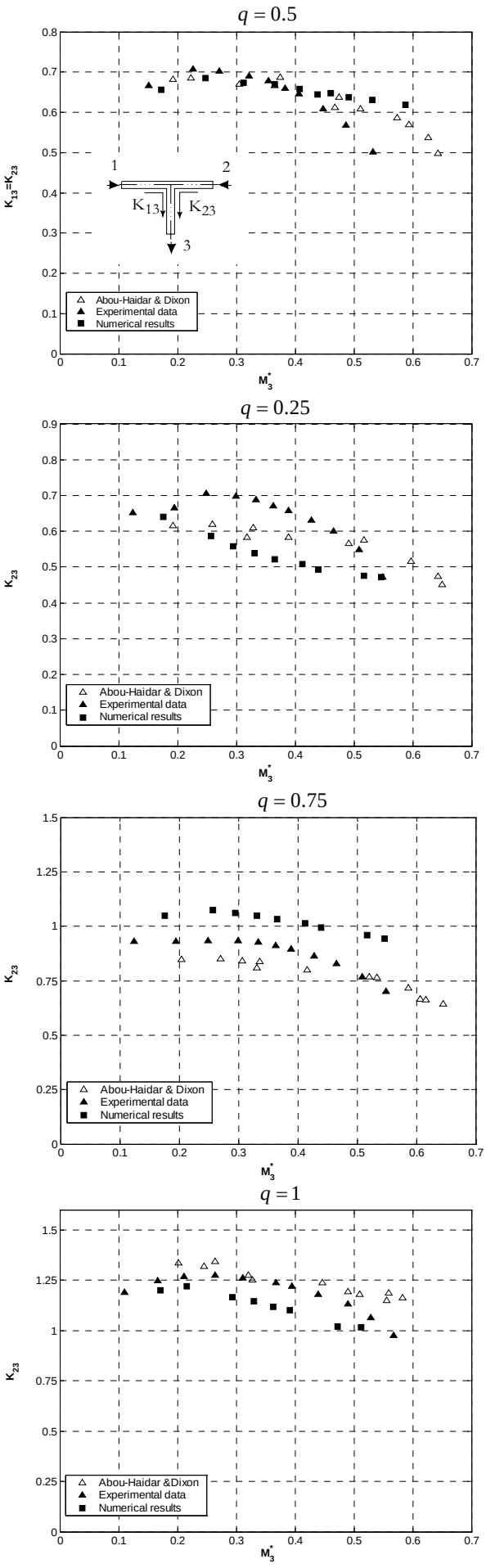

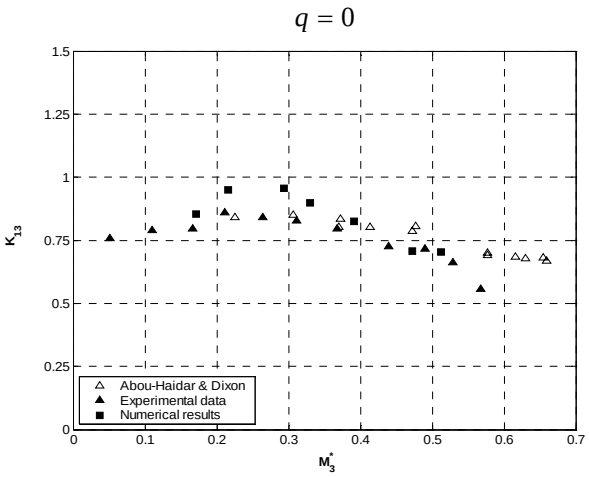

Figure 10. Compressible flow loss coefficients K_{23}, comparison among Abou-Haidar and Dixon's data, experimental data and numerical results. Combining flow type $C2$

At $q=1$ a satisfactory agreement is achieved. The maximum discrepancies are about $\pm 10\%$. The numerical results are slightly overestimated at $q=0.75$ and underestimated at $q=0.25$. This fact can be due to the complexity to establish the mass flow rate ratio accurately in the experimental test, while numerically this ratio is fixed by boundary conditions. In all cases, the discrepancies are within the calculated total uncertainty interval. At $q=0$ the experimental data and reference data are in good agreement and a satisfactory agreement was also obtained for the numerical results, although, less accurate predictions can be expected due that the recommended interval value of y^+ in this branch is not verified. So, a higher scattering is obtained at low extrapolated Mach numbers.

3.2.3 Dividing Flow Type $D2$

In figure 11 the results obtained at dividing flow type $D2$ are compared with Abou-Haidar and Dixon's data. In general a satisfactory agreement is obtained in all mass flow rate ratios analyzed. The Mach number interval in experimental data is strongly limited by the branch lengths and the Coriolis mass flow meter installed downstream of the junction tested. In the numerical simulations this range can be extended up to $M_3^* \approx 0.8$ at $q=0.5$.

It can be observed that the experimental and reference data are in a good agreement at $q=0.5$. However the loss coefficient obtained departing from numerical results is underestimated about 15% in the $0.2 \le M_3^* \le 0.6$ interval Mach number. This error is within the total uncertainty interval obtained for this coefficient definition, in which the measurement uncertainties are amplified, mainly the uncertainty associated to the static pressure measurement.

In the rest of mass flow rate ratios represented, the interval of extrapolated Mach number is similar in the experimental test and in the numerical simulations. At $q=1$ and $q=0.25$, an excellent agreement is achieved in all Mach numbers interval studied, although Abou-Haidar and Dixon predict a slight rise of the loss coefficient when the Mach number is increased, while the loss coefficient obtained experimentally and numerically are maintained almost constant.

At $q=0.75$, the numerical and experimental results are coincident with reference data al low Mach number, however they are slightly overestimated with respect to Abou-Haidar and Dixon's data when the Mach number is increased. The maximum discrepancies are about $\pm 10\%$. The numerical results obtained at $q=0$ are in disagreement, although the trend is similar to the experimental results. These discrepancies can be due to errors in the numerical simulation, since the model is inefficient to reproduce the complex suction effect in the branch with mass flow rate null.

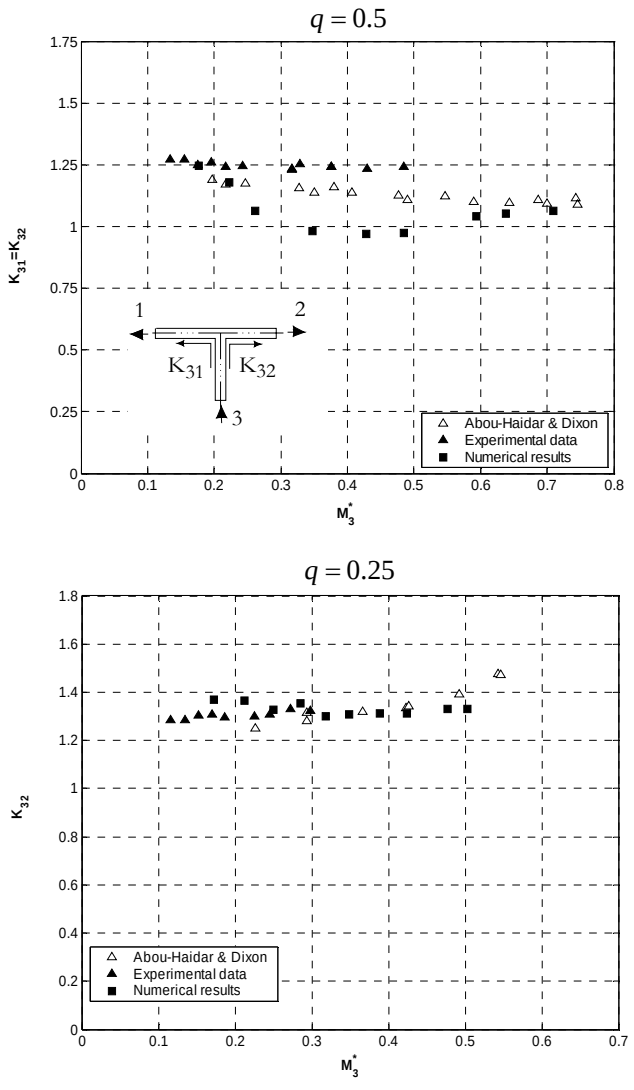

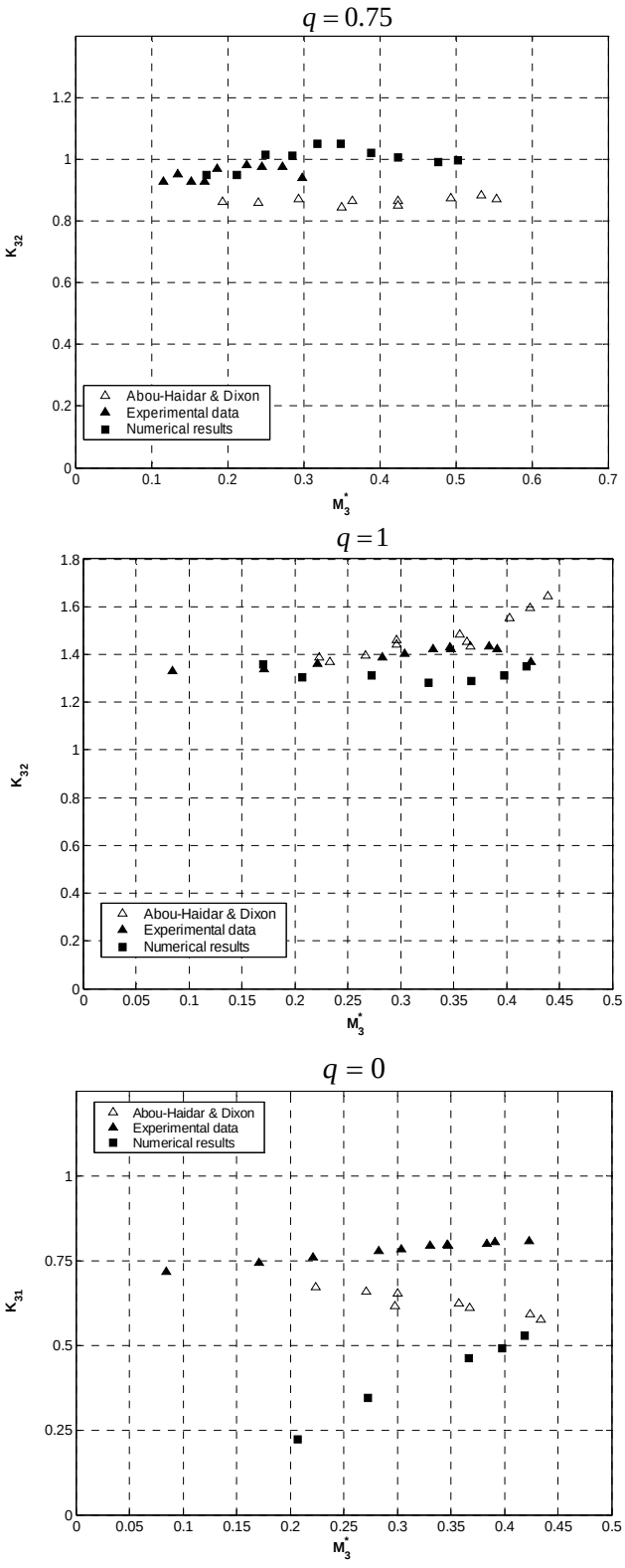

Figure 11. Compressible flow loss coefficient K_{32}, comparison among Abou-Haidar and Dixon's data, experimental data and numerical results. Dividing flow type $D2$

Finally, in table 1, practical correlations between predicted loss coefficient and mass flow rate ratio for incompressible flow are presented. In compressible flow,

correlations between predicted total pressure loss coefficient defined by Miller and the extrapolated Mach number in common branch for different mass flow rate ratios are also exposed at flow type $C2$ in table 2 and at flow type $D2$ in table 3. These correlations are used as boundary conditions in 1D global simulation models of fluid systems in which junctions are present.

In general we have obtained better correlations for the intermediate mass flow rate ratios $q = 0.75$, $q = 0.5$ and $q = 0.25$. However, at $q = 0$ and $q = 1$ the numerical results present inaccuracies due to that the turbulence model conditions are not verified in all computational domain, and a higher dispersion in the calculation of loss coefficient is propagated, such as has been explained previously.

Correlations for incompressible flow: $K = f(q) \quad q = G_2/G_3$	
Flow Type C2	**Flow Type D2**
$K_{23} = 1.264q^2 - 0.8232q + 0.8176 \quad (r^2 = 0.871)$	$K_{32} = -1.8314q^2 + 2.8887q + 0.2784 \quad (r^2 = 0.9919)$
$K_{13} = 1.264q^2 - 1.7048q + 1.2584 \quad (r^2 = 0.871)$	$K_{31} = -1.8314(1-q)^2 + 0.7741(1-q) + 1.3358 \quad (r^2 = 0.9919)$

Table 1. Correlations for incompressible flow

Correlations for compressible flow: $K = f(M_3^*) \quad q = Cte$ **Flow Type C2**		
$q = 1$	$K_{23} = 0.9538M_3^{*2} + 0.0237M_3^* + 1.2393$	$(r^2 = 0.9699)$
$q = 0.75$	$K_{23} = -1.1611M_3^{*2} + 0.5101M_3^* + 1.0051$	$(r^2 = 0.9725)$
$q = 0.5$	$K_{23} = K_{13} = -0.5661M_3^{*2} - 0.2988M_3^* + 0.6317$	$(r^2 = 0.8706)$
$q = 0.25$	$K_{23} = 0.8662M_3^{*2} - 1.0831M_3^* + 0.8041$	$(r^2 = 0.9983)$
$q = 0$	$K_{13} = -4.9536M_3^{*2} + 2.8296M_3^* + 0.5119$	$(r^2 = 0.8292)$

Table 2. Correlations for compressible flow. Flow type C2

Correlations for compressible flow: $K = f(M_3^*) \quad q = Cte$ **Flow Type D2**		
$q = 1$	$K_{32} = 4.1327M_3^{*2} - 2.4865M_3^* + 1.6579$	$(r^2 = 0.7823)$
$q = 0.75$	$K_{32} = 1.3878M_3^{*2} - 1.1025M_3^* + 1.5273$	$(r^2 = 0.7551)$
$q = 0.5$	$K_{32} = K_{31} = 2.7262M_3^{*2} - 2.6427M_3^* + 1.6058$	$(r^2 = 0.89)$
$q = 0.25$	$K_{32} = -2.6801M_3^{*2} + 1.933M_3^* + 0.6862$	$(r^2 = 0.7735)$
$q = 0$	*Numerical results do not provide a good correlation in this case*	

Table 3. Correlations for compressible flow. Flow type D2

4. Conclusions

A validated processing methodology departing from numerical results obtained with the general purpose package software Fluent has been developed. This procedure uses the one-dimensional Fanno model to obtain the friction coefficient and subtract the frictional losses from the total energy losses of the fluid flow. Once the extrapolated properties up to the junction are calculated, the total pressure loss coefficient in 3D steady compressible flow at junctions can be computed.

The methodology has been validated comparing the loss coefficient obtained at 90 degree T-type junction by numerical simulation with experimental data and reference data available in open literature, in incompressible and compressible forms. The predicted and experimental data show, in general, a good agreement with reference data, both in combining and dividing flow types and for different mass flow rate ratios between branches, taking into account the different procedures utilized.

The interval of extrapolated Mach numbers simulated is mainly influenced by branch lengths of the junction, since the choked flow conditions due to frictional losses is reached at a lower mass flow rate when the branch length is longer. In this way, the branch lengths must be as short as possible, however, to obtain fully-developed flow conditions, great L/D ratios are required.

It has been found that careful experiments are needed to obtain reliable experimental data in compressible flow and that CFD can be applied to yield accurate predictions. The RANS based turbulence model which agrees best with experimental and reference data is the $k-\omega$ SST when a coupled implicit solver is used. In addition, the numerical simulations allow understanding the internal structure of the complex flow inside junctions.

The experimental tests have been optimized. So, the required measurement locations were only one at each branch, and the main source of uncertainty of measurement has been minimized using Coriolis mass flow meters. The processing methodology of experimental data is based on the one-dimensional steady adiabatic compressible flow model to extrapolate the properties up to the junction. The non-dimensional friction coefficient is obtained in this case from von Karman-Nikuradse or Colebrook-White correlations assuming fully-developed and uniform flow conditions. These last conditions are difficult to achieve and demand a well studied placing of measurement section, this decision can be assisted through numerical simulation.

The definition of loss coefficient used in the comparisons shows, in general, a small sensitivity in relation to extrapolated Mach number variations and the uncertainty propagation of measurements in the result is up to about ±25% in some flow types. Hence this loss coefficient definition could be optimized for compressible flow. It is interesting to emphasize that the developed methodology can be applied to other complex geometries, such as, T-type junctions with different lateral branch angles, Y-type junctions, junctions with different area ratios between branches or with area variation along the branches.

Finally, the loss coefficients obtained for different mass flow rate ratios applying this methodology will allow us to obtain correlations that can be used as boundary conditions in one-dimensional global simulation models.

Acknowledgements

This research has been supported by the Seneca project PB/19/FS/97 Comunidad Autónoma Región de Murcia (experimental facilities) and MCYT project DPI2003-02719 (software). The numerical simulations have been made in the computer facilities at the SAIT (Universidad Politécnica de Cartagena).

REFERENCES

[1] M.D. Basset, D.E. Winterbone, R.J. Pearson, Modelling engines with pulse converted exhaust manifolds using one-dimensional techniques, SAE paper 2000-01-0290, 2000

[2] T. Bulaty, M. Widenhorn, Unsteady flow calculation of sophisticated exhaust systems using a multibranch junction model, Journal of Engineering for Gas Turbines and Power, ASME (1993) Vol 115 pp. 756,760

[3] G. Chiatti, O. Chiavola, Multicode prediction of the influence of the exhaust system on the performance of a turbocharged engine, Journal of Engineering for Gas Turbines and Power, ASME, July (2002) Vol 124 Issue 3 pp. 695-701

[4] D.S Miller, Internal Flow – a guide to losses in pipe and duct systems-, 2nd ed., BHRA, 1971

[5] ESDU 73022, 1973, Pressure losses coefficients in three-leg pipe junctions: dividing flows, ESDU International plc,. London

[6] ESDU 73023, 1973, Pressure losses coefficients in three-leg pipe junctions: combining flows, ESDU International plc., London

[7] H. Ito, K. Imai, Energy losses at 90º pipe junctions. Journal of Hydraulic Division. HY9 (1973) pp. 1353-1369

[8] R.S. Benson, D. Woollatt, W.A. Woods, Unsteady flow in simple branch systems, Proc. Instn. Mech. Eng., Paper 10, Vol 178 Pt 3I(iii), 1964, pp. 285-296

[9] A. Dadone, Perdite di carico nelle giuzinoni, ATA 26, (1973) pp. 214-224

[10] T. Morimune, N. Hirayama, T. Maeda, Study of compressible high speed gas flow in piping system, Bulletin of the JSME, Vol. I24, Nº 198, (1981) pp. 2082-2089

[11] N.I. Abou-Haidar, S.L. Dixon, Pressure losses in combining subsonics flows through branched ducts. Trans. ASME, Journal of Turbomachinery, Vol. 114, Nº 1, (1992) pp. 264-270

[12] M.D. Basset, R.J. Pearson, D.E. Winterbone, R. Sierens, Steady-flow loss-coefficient estimation for exhaust manifold pulse-converter type junctions, paper SAE 1999-01-0213, 1999

[13] W.H. Hager, An approximate treatment of flow in branches and bends, Procc. Inst. Mech. Eng. Vol 198C, Nº 4, (1984) pp. 63-69

[14] D.E. Winterbone, R.J. Pearson, Theory of engine manifold design. Wave action methods for IC engines. Professional Engineering Publishing. London, 2000

[15] M.A. Leschziner, K.P. Dimitriadis, Computation of three-dimensional turbulent flow in non-orthogonal junctions by a branch-coupling method, Computer & Fluids, Vol 17, Nº 2, 1989, pp. 371-396

[16] H. Fu, M.J. Tindal, A.P. Watkins, M. Yianneskis, Computation of three-dimensional turbulent flows in a pipe junction with reference to engine inlet manifolds, Proc. Instn. Mech. Eng., Vol 206 C02192, (1992) pp. 285-296

[17] T.W. Kuo, S. Chang, Three-dimensional steady flow computations in manifold-type junctions and a comparison with experiment, Paper SAE 932511, 1993

[18] T.W. Kuo, B. Khaligi, Numerical study on flow distribution in T-junctions and comparison with experiment. Trans ASME, ICE Vol 23 Eng. modelling (1995) pp. 8-31

[19] Y. Zhao, D.E. Winterbone, A study of multi-dimensional gas flow in engine manifolds, Proc. Inst. Mech. Eng., Vol 218, Part C, D04892, 1994

[20] C.T. Shaw, D.J. Lee, S.H. Richardson, S. Pierson, Modelling the effect of plenum-runner interface geometry on the flow through an inlet system, Paper SAE 2000-01-0569, 2000

[21] G. Gan, S.B. Riffat, Numerical determination of energy losses at duct junctions, Applied energy, 67, (2000) pp. 331-340

[22] U. Kesgin, Study on the design of inlet and exhaust system of a stationary internal combustion engine, Energy Conversion and management, 46, (2005) pp. 2258-2287

[23] D.S. Miller, Compressible Internal Flow, Vol 10 Fluid Eng. Series BHRA, (1984)

[24] A. Christian, A. Selamet, K.D. Miazgowicz, K.V. Tallio, Flow losses at circular T-junctions representative of intake plenum and primary runner interface, (2004) Paper SAE 2004-01-1414

[25] F.R. Menter, Improved Two-Equation $k-\omega$ Turbulence Models for Aerodynamic Flows, NASA TM-103975, (1992)

[26] D. Wilcox, Turbulence modelling for CFD. DCW Industries, Inc., Griffin printing, California, (2000)

[27] Manual Fluent v 6 .2

[28] E. Sanmiguel-Rojas, J. Ortega-Casanova, C. Del-Pino-Peñas, R. Fernandez-Feria, A Cartesian grid finite-difference method for 2D incompressible viscous flows in irregular geometries. Journal of Computational Physics, 204 (2005) 302-318

[29] Guide to the Expression of Uncertainty in Measurement, ISO, 1993